NJC

Accepted Manuscript

This is an *Accepted Manuscript*, which has been through the Royal Society of Chemistry peer review process and has been accepted for publication.

Accepted Manuscripts are published online shortly after acceptance, before technical editing, formatting and proof reading. Using this free service, authors can make their results available to the community, in citable form, before we publish the edited article. We will replace this *Accepted Manuscript* with the edited and formatted *Advance Article* as soon as it is available.

You can find more information about *Accepted Manuscripts* in the Information for Authors.

Please note that technical editing may introduce minor changes to the text and/or graphics, which may alter content. The journal's standard Terms & Conditions and the Ethical guidelines still apply. In no event shall the Royal Society of Chemistry be held responsible for any errors or omissions in this *Accepted Manuscript* or any consequences arising from the use of any information it contains.

ROYAL SOCIETY OF CHEMISTRY

www.rsc.org/njc

Facile Electrochemical Synthesis of CeO_2 Hierarchical Nanorods and Nanowires with Excellent Photocatalytic Activities

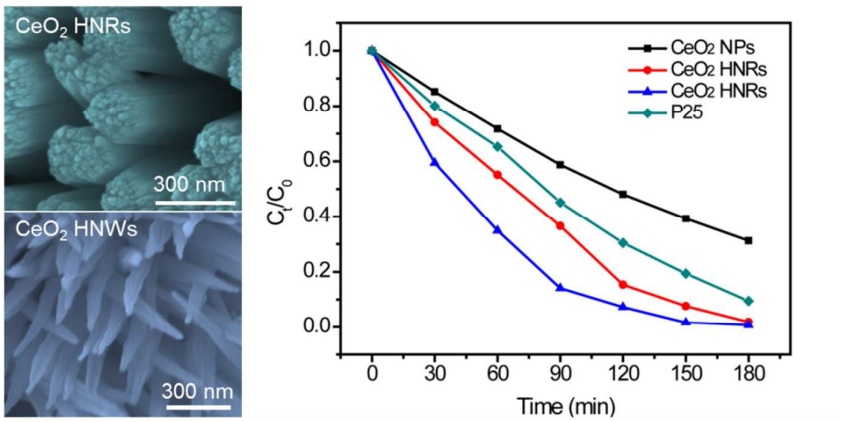

A simple, cost-effective and controllable electrochemical method has been developed to synthesize free-standing CeO_2 hierarchical nanorods and nanowires.

Journal Name

RSCPublishing

ARTICLE

Facile Electrochemical Synthesis of CeO_2 Hierarchical Nanorods and Nanowires with Excellent Photocatalytic Activities

Cite this: DOI: 10.1039/x0xx00000x

Received 00th January 2012,
Accepted 00th January 2012

DOI: 10.1039/x0xx00000x

www.rsc.org/

Chao Zhang,[a] Xiyue Zhang,[a] Yichen Wang,[a] Shilei Xie,[a] Yi Liu,[b] Xihong Lu,[a]* and Yexiang Tong[a]

In this work, we developed a simple, cost-effective and controllable electrochemical method to synthesize free-standing CeO_2 hierarchical nanorods and nanowires. Due to the hierarchical one-dimensional nanostructures and increased surface areas, both the CeO_2 hierarchical nanorods and nanowires exhibit substantially higher photocatalytic performance than the commercial CeO_2 nanoparticles in the degradation of methyl orange.

Introduction

Rare earth oxides, one of the most important families of rare-earth materials, are a particularly interesting class of materials because of their unique optical, electronic, magnetic, and catalytic properties arising from the confinement of the 4f electrons. [1] These unique properties are crucial for many practical applications, such as optical communication, optical displays, efficient catalysis, UV shielding, and medical diagnostics. [2-6] As one of the most functional rare earth oxides, CeO_2 has attracted numerous attentions due to its excellent physical and chemical properties and wide applications in catalysts, fuel cells, UV blockers, solar cells, oxygen storage capacitors and sensors. [7-11] It is widely known that the photocatalytic, magnetic, electronic, and catalytic properties of CeO_2 are strongly size/shape dependent at the nanometer scale. [9, 12, 13] In this regard, considerable effort has been made to the design and synthesis of CeO_2 nanomaterials with controllable morphology and large surface area. [14-19] Among various nanostructures, one-dimensional (1D) CeO_2 nanostructures, such as nanorods, nanotubes, and nanowires have stimulated intensive interest because of their unique optical, electronic, and mechanical properties and potential applications in the fabrication of nanoscale devices. [12, 20-23] On the other hand, the assembly of 1D nanostructure into an appropriate hierarchical/super-structures has become the focus of research in recent years because they exhibit superior properties than the pristine 1D nanostructure. [24-27] For instance, compared with randomly dispersed nanorods, the highly ordered nanorod superstructures can allow for heterostructures, have larger surface areas, and can form continuous networks. [28] Therefore, once the nanorods as building blocks can be rationally assembled into appropriate three-dimensional (3D) superstructures, they will offer new scientific opportunities for investigating the influence of size and dimensionality with respect to their collective optical, magnetic, and electronic properties. [24, 29] Up to now, some CeO_2 hierarchical nanostructures such as hierarchical nanospheres, [30, 31] nanoflowers [32-34] and urchin-like structure [35] have been reported. Despite these achievements, a simple and efficient method for synthesizing shape-controlled CeO_2 1D hierarchical nanostructures is still lacking.

Electrochemical deposition technique has been widely recognized as a promising alternating candidate for the preparation of nanomaterials because of its low cost, rapidness, environmentally friendly and potential advantage for large-scale production. [36-38] Moreover, the operational conditions (applied current or potential, composition of the electrolyte) usually allow to modify and control the deposit morphology through changes of mass transport and (electro-)crystallization phenomena. [37, 39-41] In recent years, electrochemical deposition technique has been also employed to the synthesis of CeO_2 nanostructures, and multifarious CeO_2 nanosturctures including nanoshperes, [31] nanorods, [12] nanowires, [42] nanotubes, [43, 44] and nanobelts [45] have been successfully synthesized by electrochemical deposition technique. Nevertheless, to the best of our knowledge, there are few reports on the preparation of CeO_2 hierarchical nanostructures via the electrochemical deposition technique so far. [17, 19, 32] In this work, we developed a facile and cost-effective electrochemical deposition method to prepare CeO_2 hierarchical nanorods (HNRs) and hierarchical nanowires (HNWs) and demonstrated their implementation as high-efficient photocatalysts for methyl orange (MO) degradation. This present electrochemical method allows us to easily manipulate the morphology and structure of the product, and free-standing CeO_2 HNRs and HNWs could be readily grown on Cu substrates by this electrochemical method. Moreover, both CeO_2 HNRs and HNWs exhibit substantially higher photocatalytic performance than the commercial CeO_2 nanoparticles (NPs) in the degradation of methyl orange (MO).

Experimental

Preparation of CeO_2 hierarchical nanorods (HNRs) and nanowires (HNWs): All reagents used in this work were of analytical grade and were used directly without any purification. All the electrochemical deposition experiments were carried out in a conventional three-electrode glass cell by galvanostatic electrolysis. The working electrode is a Cu foil of 1.5 cm × 3 cm, while the counter electrode and reference electrode is a graphite rod of about 4.0 cm^2 and a saturated Ag/AgCl electrode, respectively. Before

electrodeposition, the Cu foil was cleaned ultrasonically in distilled water, ethanol, and acetone and then rinsed in distilled water again. Electrodeposition of CeO_2 HNRs were performed in solution of 0.01 M $Ce(NO_3)_3$ + 0.1 M NH_4Cl+0.05 M KCl with a current density of 0.44 mA cm^{-2} for 2 h at 70 ^oC, while that of HNWs were carried out in the same electrolyte with a current density of 0.88 mA cm^{-2} for 2 h at 70 ^oC.

Structural and componential Characterizations: The morphology and structure of products were characterized by scanning electron microscope (SEM, Quanta 400), X-ray diffraction (XRD, Bruker, D8 ADVANCE) and transmission electron microscopy (TEM, JEM2010-HR). The composition and surface oxidation states of products were studied by X-ray Photoelectron Spectroscopy (XPS, ESCALab250) with 200 W Al KR radiation in twin anode. The optical properties of the products were measured with a UV-Vis-NIR Spectrophotometer (UV, Shimadzu UV-3150). The BET surface area of samples was characterized by nitrogen adsorption/desorption isotherms at 77 K that conducted on an ASAP 2020 V3.03 H instrument. All the samples (powders) were outgassed at 100 ^oC for 300 min under flowing nitrogen before measurements. For the SEM, XRD and UV-spectra of CeO_2 samples, measurements were directly carried out on the samples without removing the Cu substrates. For the measurements of the TEM, BET and photocatalytic methyl orange (MO), CeO_2 films were exfoliated and ground into powders, then used the powders for these tests.

Photocatalytic tests: Photocatalytic properties of the CeO_2 HNRs and HNWs were evaluated using methyl orange (MO) as a demonstration dye under Xe lamp (500 W, Beijing Changtuo, PLSLAX500, wavelength: 200-800 nm) irradiation at room temperature with cooling water. Typically, 20 mg of CeO_2 samples (powders) was suspended in 100 ml of 20 mg/L MO aqueous solution (pH = 3). The suspension was magnetically stirred in the dark for 24 h to ensure establishment of an adsorption-desorption equilibrium before light irradiation. Then, at different light irradiation intervals, 3 ml of the suspensions was collected, filtered through a 0.45 lm membrane, and finally analyzed by a Shimadzu UV-3150a UV-Vis-NIR Spectrophotometer immediately.

Results and discussion

Electrodeposition of CeO_2 HNRs was performed in solution of 0.01 M $Ce(NO_3)_3$ + 0.1 M NH_4Cl+0.05 M KCl with a current density of 0.44 mA cm^{-2} for 2 h at 70 ^oC. Figure 1 displays the typical scanning electron microscopy (SEM) images of the CeO_2 HNRs. It can be clearly observed that CeO_2 flower-like nanostructures consisting of high density nanorods were successfully grown on Cu substrates. These CeO_2 nanorods are very uniform and have a diameter of around 200-250 nm. More interestingly, the CeO_2 nanorods were constructed by a large number of CeO_2 nanowires with a small size (Figure 1c). To identify the crystalline phase of the product, X-ray diffraction (XRD) spectrum of CeO_2 HNRs was collected and shown in Figure 1d. Besides the Cu peaks coming from the Cu substrates, all of the peaks in the XRD spectrum can be well indexed to a fluorite cubic structure of CeO_2 (JCPDF # 65-2975) with lattice constants a = 0.5411 nm. No any other peaks were detected, indicating the product is highly pure. Additionally, the relative strong intensity of CeO_2 peaks suggests the CeO_2 HNRs possess a good crystallinity.

To investigate the microstructure of CeO_2 HNRs, transmission electron microscopy (TEM) analysis was performed. Figure 2a is a typical TEM image of a single CeO_2 HNR, clearly showing the diameter of the nanorod is about 200 nm, which is in accordance with the SEM result. The enlarged TEM image (inset in Figure 2a) reveals this CeO_2 nanorod was made up of numerous nanowires. The

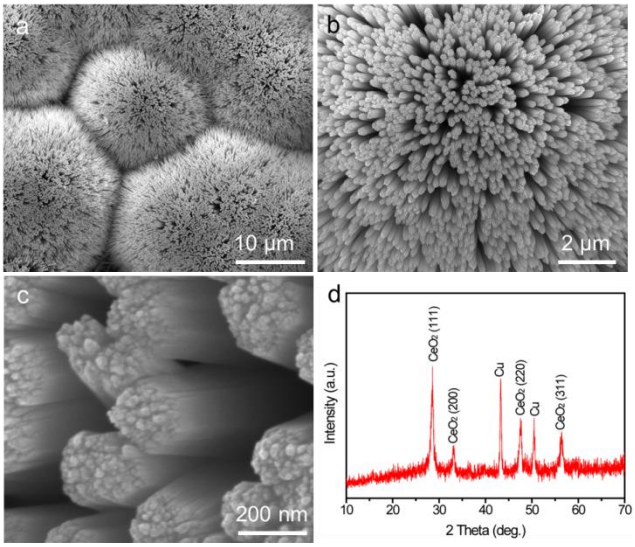

Figure 1. (a-c) SEM images and (d) XRD spectrum of CeO_2 HNRs prepared with a current density of 0.44 mA cm^{-2}.

corresponding select area electron diffraction (SAED) pattern of this CeO_2 nanorod is inserted in Figure 2a. The bright diffraction spots confirm the highly crystalline nature of this nanorod, and more evidences can be seen from the HRTEM observation.[15] Figure 2b presents the high-resolution TEM (HRTEM) image of the CeO_2 nanorod. The well-resolved two-dimensional lattice fringes again confirm that the CeO_2 nanorod has a high crystallinity.[15, 18] The lattice fringe with a d-spacing of 0.31 nm matches well with the (111) interplanar spacing of face-centered-cubic CeO_2.

X-ray photoelectron spectroscopy (XPS) analysis was also conducted to further study the composition of CeO_2 HNRs. The XPS survey spectrum of CeO_2 HNRs is presented in Figure 3a. Only Ce, C and O signals are observed on the surface of the sample, which indicates the high purity of the CeO_2 HNRs because the C single originates from the adventitious carbon. Figure 3b displays the Ce 3d core level XPS spectrum of CeO_2 HNRs, which can be deconvolved to eight peaks. The peaks labeled as v_1 and u_1 are the characteristic peaks of Ce^{3+} states while others are the characteristic peaks of Ce^{4+} states. [46] This result indicates that Ce^{4+} ions are dominant in the deposit and a small quantity of Ce^{3+} is also present in this deposit. Figure 3c shows the O 1s core level XPS spectrum of CeO_2 HNRs, which can be deconvolved into two peaks. The peak centered at 529.4 eV is assigned to the oxygen bond of Ce–O–Ce, and the peak located at 531.3 eV corresponds to Ce–O–H, respectively. [47] The XPS results mentioned above reveal that the as-deposited product is mainly CeO_2, which consists with the XRD and TEM analyses. [20, 45]

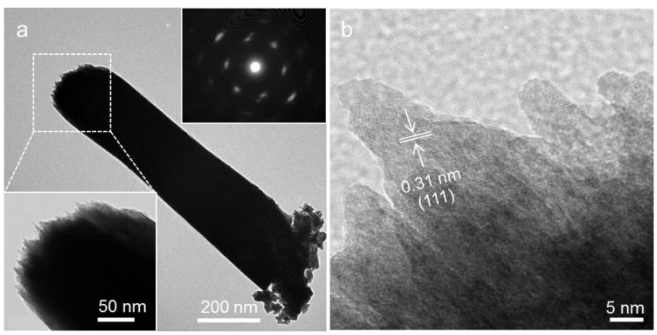

Figure 2. (a) TEM image and (b) HRTEM image of the CeO_2 nanorods. The insets are the enlarged TEM image and corresponding SAED pattern.

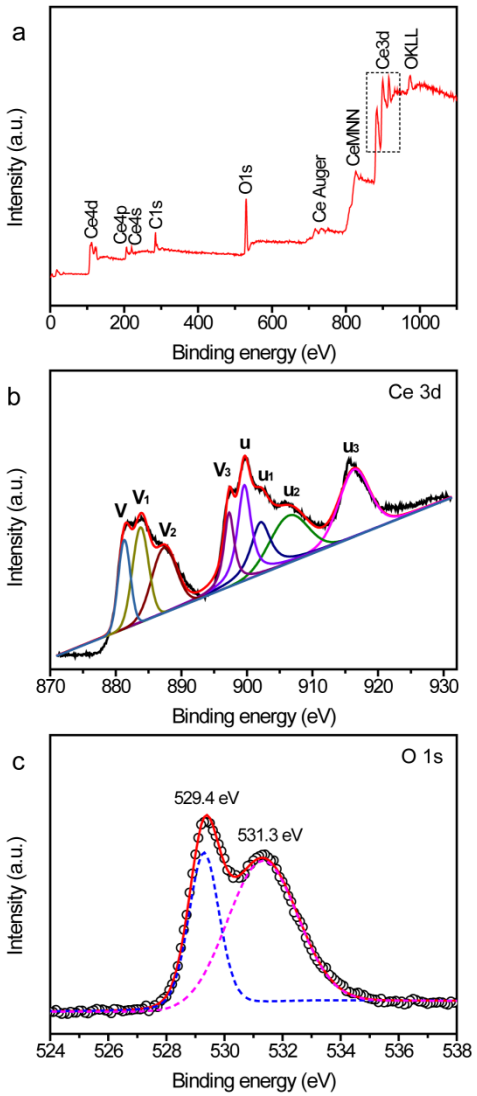

Figure 3. (a) XPS survey spectrum, (b) Ce 3d core level XPS spectrum and (c) O 1s core level XPS spectrum of the as-prepared CeO_2 HNRs.

Our present electrochemical method allows further structural manipulation. As shown in Figure 4a, a new kind of the CeO_2 spear-like hierarchical nanowires (denoted as HNWs) was successfully obtained when simply increased the deposition current density to 0.88 mA cm^{-2}. The enlarged SEM images show that these CeO_2 HNWs with a diameter of about 100 nm vertically grew on Cu substrates (Figure 4b and the inset). A typical TEM image of single CeO_2 HNW is shown in Figure 4c. The spear-like morphology of the HNW is distinctly observed, and the diameter of this HNW (measured in middle) is about 80 nm. Figure 4d is the enlarged TEM image taken from the red rectangle part of the HNW (Figure 4c), showing this HNWs was composed of several small size nanowires (indicated by red arrows). Figure 4e displays the HRTEM image of CeO_2 HNW taken from the red circle part. The well-resolved lattice fringes clearly demonstrate that the CeO_2 HNW also has a high degree of crystallinity. The lattice fringe with the spacing of 0.31 nm corresponds to the interplanar spacing of (111) plane spacing of cubic CeO_2. Additionally, SAED analysis confirms the CeO_2 HNW is highly crystalline (inset in Figure 4e).

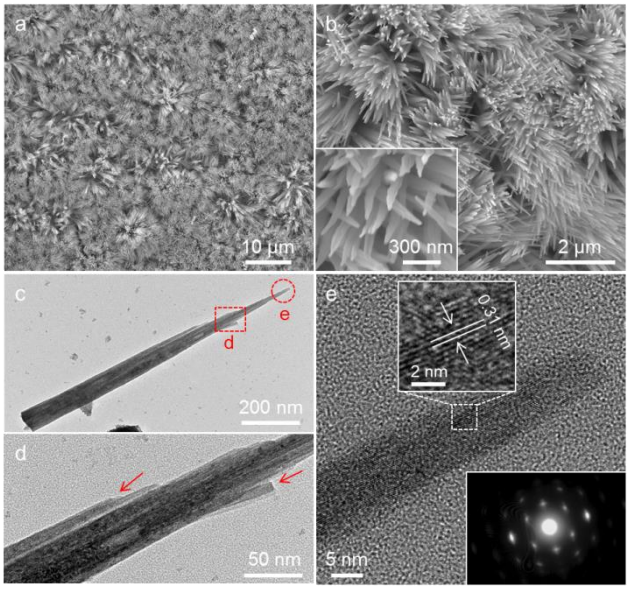

Figure 4. (a-b) SEM images, (c, d) TEM images and (e) HRTEM image of CeO_2 HNWs prepared with a current density of 0.88 mA cm^{-2}. The insets in Figure 4e are the enlarge HRTEM image and the corresponding SAED pattern.

Figure 5a shows the nitrogen adsorption–desorption isotherms of the CeO_2 HNRs and HNWs collected at 77 K. Both the CeO_2 HNRs and HNWs exhibited typical Langmuir IV characteristic with an obvious hysteresis loop, suggesting that there are mesopores in CeO_2 HNRs and HNWs. The specific surface areas of CeO_2 HNRs and HNWs calculated by the Brunauer-Emmett-Teller (BET) method are 58.6 and 69.4 m^2 g^{-1}, respectively. Figure 5b shows the UV-visible absorption spectra of the CeO_2 HNRs and HNWs. Both the samples exhibited a similar absorption band edge at about 390 nm, which is consistent with the CeO_2 band-gap of 3.2 eV. [7, 12] In comparison to the CeO_2 HNRs, the CeO_2 HNWs displays higher absorption in the wavelength range between 400 and 750 nm, suggesting the CeO_2 HNWs could utilize visible light.

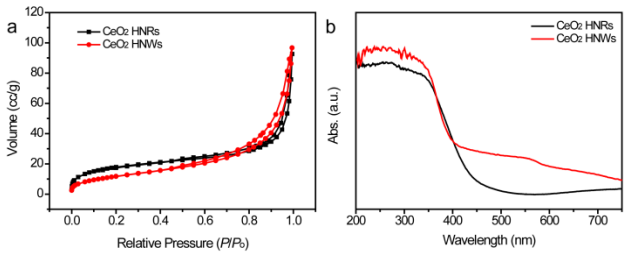

Figure 5. (a) Nitrogen adsorption–desorption isotherms of the CeO_2 HNRs and HNWs at 77 K.

To study the photocatalytic activities of the as-prepared CeO_2 samples, the efficiencies of photocatalytic degradation of MO under light irradiation were measured. For better comparison, commercial CeO_2 nanoparticles (NPs) and TiO_2 nanoparticles (P25, Degussa) were also examined in the same test. Before the photocatalytic tests, the CeO_2 samples were magnetically stirred in the dark for 12 h to reach the adsorption−desorption equilibrium. Figure 6 compares the photodegradation efficiencies of MO as a function of irradiation time for different samples. The y-axis was defined as C_t/C_0, where C_t was the main absorption peak intensity of MO sampled at each irradiated time interval and C_0 was the absorption intensity of the starting concentration. Significantly, both the CeO_2 HNRs and HNWs

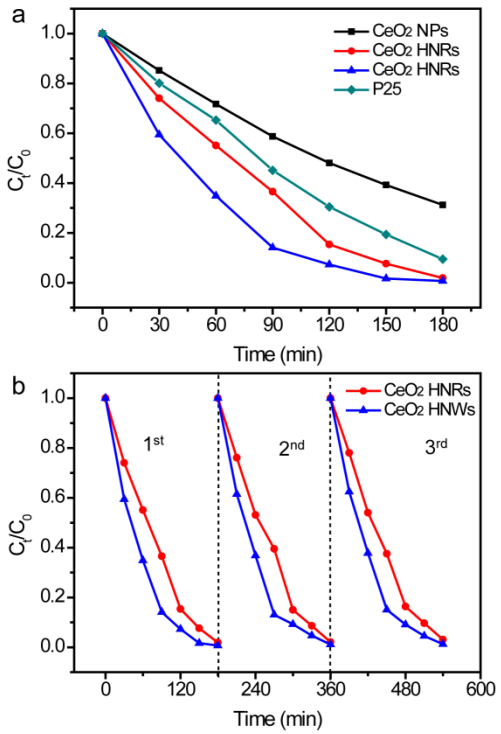

Figure 6. (a) Photodegradation efficiencies of MO for commercial CeO_2 NPs, P25, CeO_2 HNRs and CeO_2 HNWs as a function of light irradiation time. (b) Cycling performance of CeO_2 HNRs and CeO_2 HNWs for MO degradation.

exhibited substantially faster degradation rate of MO than the commercial CeO_2 NPs and P25. After 180 min light irradiation, the photocatalytic degradation efficiencies of MO solution for CeO_2 HNRs and HNWs achieved 98.2% and 99.3%, while the commercial CeO_2 NPs and P25 only reached 68.8% and 89.5% respectively. Moreover, the CeO_2 HNRs and HNWs have good cycling stability. As shown in Figure 6b, both the CeO_2 HNRs and HNWs exhibited no any decay of their photocatalytic activities after three cycles. The BET surface area of CeO_2 HNRs (58.6 m^2 g^{-1}) and HNWs (69.4 m^2 g^{-1}) is higher than the commercial CeO_2 NPs (50.2 m^2 g^{-1}). Additionally, these hierarchical 1D nanorods and nanowires not only can provide large interface areas for photocatalytic reaction, but also shorten the diffusion pathway for minority carriers. [48-50] Therefore, such superior photocatalytic performances of CeO_2 HNRs and HNWs are mainly attributed to their hierarchical 1D nanostructures and higher surface areas. On the other hand, compared to the CeO_2 HNRs, the CeO_2 HNWs show a faster degradation rate of MO. As indicated by Figure 5b, the CeO_2 HNWs have stronger absorption than the CeO_2 HNRs in visible light region, and hence the CeO_2 HNWs may absorb more light and generate more electrons and holes than the CeO_2 HNRs at the same time. The superior photoactivity of CeO_2 HNWs than the HNRs is due to its larger surface area and improved light-harvesting ability.

Conclusions

In summary, free-standing CeO_2 HNRs and HNWs were successfully synthesized on Cu substrates by a simple, low cost and environmentally friendly electrochemical deposition approach. The morphology and structure of the products can be readily controlled by simply adjusting the current density. Furthermore, both the CeO_2 HNRs and HNWs could remove 98.2% and 99.3% of MO under light irradiation for 180 min, which is substantially higher than the commercial CeO_2 NPs (68.8%) and P25 (89.5%). The superior photocatalytic performance can be attributed to their increased surface areas and hierarchical 1D nanostructures that provide more active sites for photocatalytic reaction and shorter diffusion length for minority carriers. This work not only demonstrates a facile electrochemical method to synthesize CeO_2 hierarchical 1D nanostructures, but also may open up new opportunities in the design and preparation of high-efficient photocatalysts.

Acknowledgements

We acknowledge the financial support from the Natural Science Foundations of China (21273290, 91323101 and J1103305), the Research Fund for the Doctoral Program of Higher Education of China (20120171110043), the Young Teacher Starting-up Research program of Sun Yat-Sen University and the Laboratory opening Fund of Sun Yat-sen University.

Notes and references

[a] MOE of the Key Laboratory of Bioinorganic and Synthetic Chemistry, KLGHEI of Environment and Energy Chemistry, School of Chemistry and Chemical Engineering, Institute of Optoelectronic and Functional Composite Materials, Sun Yat-Sen University, Guangzhou 510275, China. E-mail: luxh6@mail.sysu.edu.cn

[b] School of Chemistry and Chemical Engineering, GuangDong Pharmaceutical University, Guangzhou 510006, China

† Footnotes should appear here. These might include comments relevant to but not central to the matter under discussion, limited experimental and spectral data, and crystallographic data.

Electronic Supplementary Information (ESI) available: [details of any supplementary information available should be included here]. See DOI: 10.1039/b000000x/

1. Z.-G. Yan and C.-H. Yan, *J. Mater. Chem.*, 2008, **18**, 5046-5059.
2. G.-y. Adachi and N. Imanaka, *Chem. Rev.*, 1998, **98**, 1479-1514.
3. R. Li, S. Yabe, M. Yamashita, S. Momose, S. Yoshida, S. Yin and T. Sato, *Mater. Chem. Phys.*, 2002, **75**, 39-44.
4. R. Li, S. Yabe, M. Yamashita, S. Momose, S. Yoshida, S. Yin and T. Sato, *Solid State Ionics*, 2002, **151**, 235-241.
5. M. V. Ganduglia-Pirovano, A. Hofmann and J. Sauer, *Surf. Sci. Rep.*, 2007, **62**, 219-270.
6. S. Yin, Y. Minamidate, S. Tonouchi, T. Goto, Q. Dong, H. Yamane and T. Sato, *RSC Adv.*, 2012, **2**, 5976-5982.
7. X. Lu, T. Zhai, H. Cui, J. Shi, S. Xie, Y. Huang, C. Liang and Y. Tong, *J. Mater. Chem.*, 2011, **21**, 5569-5572.
8. C. W. Sun, H. Li and L. Q. Chen, *Energy Environ. Sci.*, 2012, **5**, 8475-8505.
9. D. Zhang, X. Du, L. Shi and R. Gao, *Dalton Trans.*, 2012, **41**, 14455-14475.
10. H. Yu, Y. Bai, X. Zong, F. Tang, G. M. Lu and L. Wang, *Chem. Commun.*, 2012, **48**, 7386-7388.
11. X. Zhao, Y. Du, W. Ye, D. Lu, X. Xia and C. Wang, *New J. Chem.*, 2013, **37**, 4045-4051.
12. X. H. Lu, D. Z. Zheng, P. Zhang, C. L. Liang, P. Liu and Y. X. Tong, *Chem. Commun.*, 2010, **46**, 7721-7723.
13. J. Zhang, H. Kumagai, K. Yamamura, S. Ohara, S. Takami, A. Morikawa, H. Shinjoh, K. Kaneko, T. Adschiri and A. Suda, *Nano Lett.*, 2011, **11**, 361-364.

14. L. González-Rovira, J. M. Sánchez-Amaya, M. López-Haro, E. Del Rio, A. B. Hungría, P. Midgley, J. J. Calvino, S. n. Bernal and F. J. Botana, *Nano Lett.*, 2009, **9**, 1395-1400.
15. X. H. Lu, X. Huang, S. L. Xie, D. Z. Zheng, Z. Q. Liu, C. L. Liang and Y. X. Tong, *Langmuir*, 2010, **26**, 7569-7573.
16. Q. Yuan, H. H. Duan, L. L. Li, Z. X. Li, W. T. Duan, L. S. Zhang, W. G. Song and C. H. Yan, *Adv. Mater.*, 2010, **22**, 1475-1478.
17. Y. Zheng, K. Liu, H. Qiao, Y. Zhang, Y. Song, M. Yang, Y. Huang, N. Guo, Y. Jia and H. You, *Crystengcomm*, 2011, **13**, 1786-1788.
18. Z. Ji, X. Wang, H. Zhang, S. Lin, H. Meng, B. Sun, S. George, T. Xia, A. E. Nel and J. I. Zink, *ACS Nano*, 2012, **6**, 5366-5380.
19. F. Meng, F. Lu, L. Wang, J. Cui and J. Lu, *Sci. Adv. Mater.*, 2012, **4**, 1018-1023.
20. G. R. Li, D. L. Qu, L. Arurault and Y. X. Tong, *J. Phys. Chem. C*, 2009, **113**, 1235-1241.
21. Z.-R. Tang, Y. Zhang and Y.-J. Xu, *RSC Adv.*, 2011, **1**, 1772-1777.
22. P. Pal, S. K. Pahari, A. Sinhamahapatra, M. Jayachandran, G. M. Kiruthika, H. C. Bajaj and A. B. Panda, *RSC Adv.*, 2013. **3**, 10837-10847.
23. R. Pérez-Hernández, G. Mondragon-Galicia, A. Allende and J. Palacios, *Phys. Chem. Chem. Phys.*, 2013, **15**, 12702-12708.
24. J. N. Tiwari, R. N. Tiwari and K. S. Kim, *Prog. Mater. Sci.*, 2012, **57**, 724-803.
25. C. Z. Yao, B. H. Wei, H. X. Ma, H. Li, L. X. Meng, X. S. Zhang and Q. J. Gong, *J. Power Sources*, 2013, **237**, 295-299.
26. B. Liu, P. Soares, C. Checkles, Y. Zhao and G. Yu, *Nano Lett.*, 2013, **13**, 3414-3419.
27. X. Luo, Z. Lou, L. Wang, X. Zheng and T. Zhang, *New J. Chem.*, 2014, **38**, 84-89.
28. S. Xie, X. Lu, T. Zhai, J. Gan, W. Li, M. Xu, M. Yu, Y.-M. Zhang and Y. Tong, *Langmuir*, 2012, **28**, 10558-10564.
29. L. S. Zhong, J. S. Hu, H. P. Liang, A. M. Cao, W. G. Song and L. J. Wan, *Adv. Mater.*, 2006, **18**, 6.
30. H. Y. Xiao, Z. H. Ai and L. Z. Zhang, *J. Phys. Chem. C*, 2009, **113**, 16625-16630.
31. X. W. Ouyang, W. Li, S. L. Xie, T. Zhai, M. H. Yu, J. Y. Gan and X. H. Lu, *New J. Chem.*, 2013, **37**, 585-588.
32. R. Yu, L. Yan, P. Zheng, J. Chen and X. Xing, *J. Phys. Chem. C*, 2008, **112**, 19896-19900.
33. J. J. Wei, Z. J. Yang, H. X. Yang, T. Sun and Y. Z. Yang, *Crystengcomm*, 2011, **13**, 4950-4955.
34. N. S. Arul, D. Mangalaraj and T. W. Kim, *Appl. Phys. Lett.*, 2013, **102**, 223115.
35. J. Wei, Z. Yang and Y. Yang, *Crystengcomm*, 2011, **13**, 2418-2424.
36. X. Lu, D. Zheng, T. Zhai, Z. Liu, Y. Huang, S. Xie and Y. Tong, *Energy Environ. Sci.*, 2011, **4**, 2915-2921.
37. G.-R. Li, H. Xu, X.-F. Lu, J.-X. Feng, Y.-X. Tong and C.-Y. Su, *Nanoscale*, 2013, **5**, 4056-4069.
38. H. Li, C. Yao, L. Meng, H. Sun, J. Huang and Q. Gong, *Electrochim. Acta*, 2013, **108**, 45-50.
39. Y. T. Kim, J. H. Han, B. H. Hong and Y. U. Kwon, *Adv. Mater.*, 2010, **22**, 515-518.
40. X. Lu, X. Huang, S. Xie, T. Zhai, C. Wang, P. Zhang, M. Yu, W. Li, C. Liang and Y. Tong, *J. Mater. Chem.*, 2012, **22**, 13357-13364.
41. H. Li, C. Chen, X. Huang, Y. Leng, M. Hou, X. Xiao, J. Bao, J. You, W. Zhang, Y. Wang, J. Song, Y. Wang, Q. Liu and G. A. Hope, *J. Power Sources*, 2014, **247**, 915-919.
42. X. H. Lu, D. Z. Zheng, J. Y. Gan, Z. Q. Liu, C. L. Liang, P. Liu and Y. X. Tong, *J. Mater. Chem.*, 2010, **20**, 7118-7122.
43. M. Xu, S. L. Xie, X. H. Lu, Z. Q. Liu, Y. Y. Huang, Y. F. Zhao, J. Q. Ye and Y. X. Tong, *J. Electrochem. Soc.*, 2011, **158**, E41-E44.
44. C.-h. Zeng, S. Xie, M. Yu, Y. Yang, X. Lu and Y. Tong, *J. Power Sources*, 2014, **247**, 545-550.
45. G.-R. Li, D.-L. Qu and Y.-X. Tong, *Electrochem. Commun.*, 2008, **10**, 80-84.
46. P. Burroughs, A. Hamnett, A. F. Orchard and G. Thornton, *J. Chem. Soc., Dalton Trans.*, 1976, 1686-1698.
47. H.-I. Chen and H.-Y. Chang, *Solid State Commun.*, 2005, **133**, 593-598.
48. I. Gonzalez-Valls and M. Lira-Cantu, *Energy Environ. Sci.*, 2009, **2**, 19-34.
49. K. Nakata and A. Fujishima, *J. Photochem. Photobiology C: Photochem. Rev.*, 2012, **13**, 169-189.
50. Y. Wang, Q. Wang, X. Zhan, F. Wang, M. Safdar and J. He, *Nanoscale*, 2013, **5**, 8326-8339.